Georgios Lazaridis, Lambrini Papadopoulou, Vasilios Melfos, and Panagiotis Voudouris. Iron oxide crusts in 2 hypogene caves in Greece. *Journal of Cave and Karst Studies*, v. 85, no. 2, p. 51-61. DOI:10.4311/2022ES0100

IRON OXIDE CRUSTS IN 2 HYPOGENE CAVES IN GREECE

Georgios Lazaridis[1,C], Lambrini Papadopoulou[1], Vasilios Melfos[1], and Panagiotis Voudouris[2]

Abstract

Iron oxide deposits in the form of crusts are examined in the field and in the laboratory with scanning electron microscopy. Samples came from two caves developed in different geological settings but assumed by previous studies to be of hydrothermal-hypogene origin. The relation of iron oxide crusts to cave wall and ceiling morphology created by the cave's primary dissolution (speleogenesis), as well as to the formation of other speleothems, is investigated. Scanning electron microscope (SEM) elemental analysis showed a high iron content (20–78 % by weight) consistent with iron oxide minerals such as goethite, hematite, magnetite, etc. Three distinct types of iron oxide crusts were identified from the four samples that were analyzed: (1) high iron content crusts with some porosity formed on the host rock surface and discontinuities, (2) high iron content (but lower than type 1) crusts, including limestone clasts and pores originating from dissolved clasts, and (3) high iron content, significantly-porous crusts that are formed by a network of filaments that indicate microbial activity. The formation of these deposits in relation to other speleothems and to dissolution events is discussed.

INTRODUCTION

Hypogenic cave formation is a special category of speleogenesis experiencing an increase in interest as more of these caves are identified globally (Klimchouk et al., 2017). These caves differ from those in classical karst that are developed by epigene (or hypergene, as defined by Dublyansky, 2014) speleogenesis because they are formed by water recharge from lower hydrostratigraphic units and sources disconnected from the adjacent surface (Klimchouk, 2017). In many of these caves, iron oxide and iron hydroxide deposits have been reported, which are in many cases the final products of sulfide oxidation (Onac and Forti, 2011). Examples of hydrothermal caves with deposits of iron oxides and hydroxides include: Iboussières Cave in France that contains spongy, microbial, ferruginous material that forms black tubes as they are deposited in vertical wall channels (Audra 2017a), Sima de la Higuera Cave in Spain, where iron-manganese coatings are found (Gázquez et al., 2012a), the inactive sulfuric-acid-speleogenetic Rhar Medjraba cave in Algeria with iron oxides having a spongy texture and in association with microbial mats (Coiffait and Quinif, 1978, cited in Audra, 2017b), the El-Balayza Caves in Egypt where iron and manganese oxides are associated with feeders (Mostafa, 2012, cited in Audra, 2017b), a number of caves in southwest Sardinia, Italy, where at least in one cave crust formation is subaerial by water films (De Waele et al., 2017); Cave of the Winds and Glenwood Caverns in Colorado, USA, where a bacteria has been reported to have deposited iron oxide/hydroxide (Luiszer, 1994; Maslyn et al., 2017); natural cavities of the karstic iron ore deposit of Warda in northern Jordan, where the authors assume a speleogenetic process for the ore deposit based on the bacterial oxidation of methane (Al-Malabeh et al., 2008), Mbobo Mkulu in South Africa, where goethite speleothems on the ceiling are formed by dripping water (Martini, 2017), caves of the Apennines Mountains, where goethite coatings are related to the presence of mineralized water (Galdenzi and Menichetti, 2017), the Buda thermal karst of Hungary, where iron hydroxide precipitates dominated by goethite are associated with cave rafts, indicating hypogene cave discharge areas (Mádl-Szőnyi et al., 2017), and caves in Germany, where siderite weathering results in carbonic acid speleogenesis and goethite deposits (Kempe, 1971; Kempe et al., 2017; and the references therein). This list is not exhaustive, and ferromanganese deposits are also known from hypergene caves (e.g. Onac et al., 1997).

Iron oxide crusts are found also in two Greek caves, Maronia Cave and Mavros Vrachos Quarry (MVQ) Cave (Fig. 1), which are considered to be related to hydrothermal speleogenesis of hypogene origin. These crusts were sampled and investigated, and their structure and composition are described and discussed according to other known cases and formation processes. Formation of other speleothems and dissolution processes are considered in order to describe their relationship to the iron oxide crusts.

CAVE DESCRIPTIONS AND SAMPLING

Maronia Cave is the largest known cave in Thrace and has been well studied from the perspective of geology, archaeology and biology (e.g., Lazaridis, 2005; Melfos et al., 2005; Pavlides et al., 2005; Sylaiou et al., 2009; Panti, 2015). It is formed in limestones of the Eocene with nummulites. The limestone unit is relatively thin and unconformably deposited on green schists above a basal Eocene conglomerate and sandstones. The nummulitic limestones mark the beginning of the

[1] School of Geology, Aristotle University of Thessaloniki, GR-54124, Thessaloniki, Greece
[2] School of Geology and Geoenvironment, National and Kapodistrian University of Athens, GR-15780, Zographou, Athens, Greece
[C] Corresponding author: geolaz@geo.auth.gr

Figure 1. Geographic location of Greek caves where iron crusts were sampled and investigated. Map from Google Earth. Western red dot, MVQ Cave. Eastern red dot, Maronia Cave. Inset, location within Greece.

Tertiary stratigraphy in the Tertiary basins of Thrace. They are slightly inclined to the west. Both the sedimentary and metamorphic rocks were intruded and overlain by Oligocene subvolcanic and volcanic rocks represented by altered andesites alternating with tuffs (Kouris, 1980; Papadopoulos, 1982; Melfos, 1995; Pavlides et al., 2005). Maronia Cave (Fig. 2) covers about 1 ha and is well decorated with several speleothem types (Lazaridis, 2005; Melfos et al., 2005). Its small-scale dissolution morphology is considered to resemble that of hypogene caves (Vaxevanopoulos and Melfos, 2010), but most forms referred to, such as cupolas, are polygenetic. Our observations of the speleothems verify that there is a significant degree of biocorrosion (Bruxelles et al., 2016; Audra et al., 2016; Audra et al., 2017; Cailhol et al., 2019) due to the large bat populations that could be responsible for the formation of cupolas and related micro-scale forms. So, only large- and meso-scale morphology of the cave and other geochemical data could be used to investigate its speleogenesis.

Figure 2. Ground plan of Maronia Cave with sampling sites Sp55, Sp56, and Sp 57 (based on Petrocheilou, 1984).

During our research in the cave for possible presence of hydrothermal calcite deposits, iron oxide crusts were

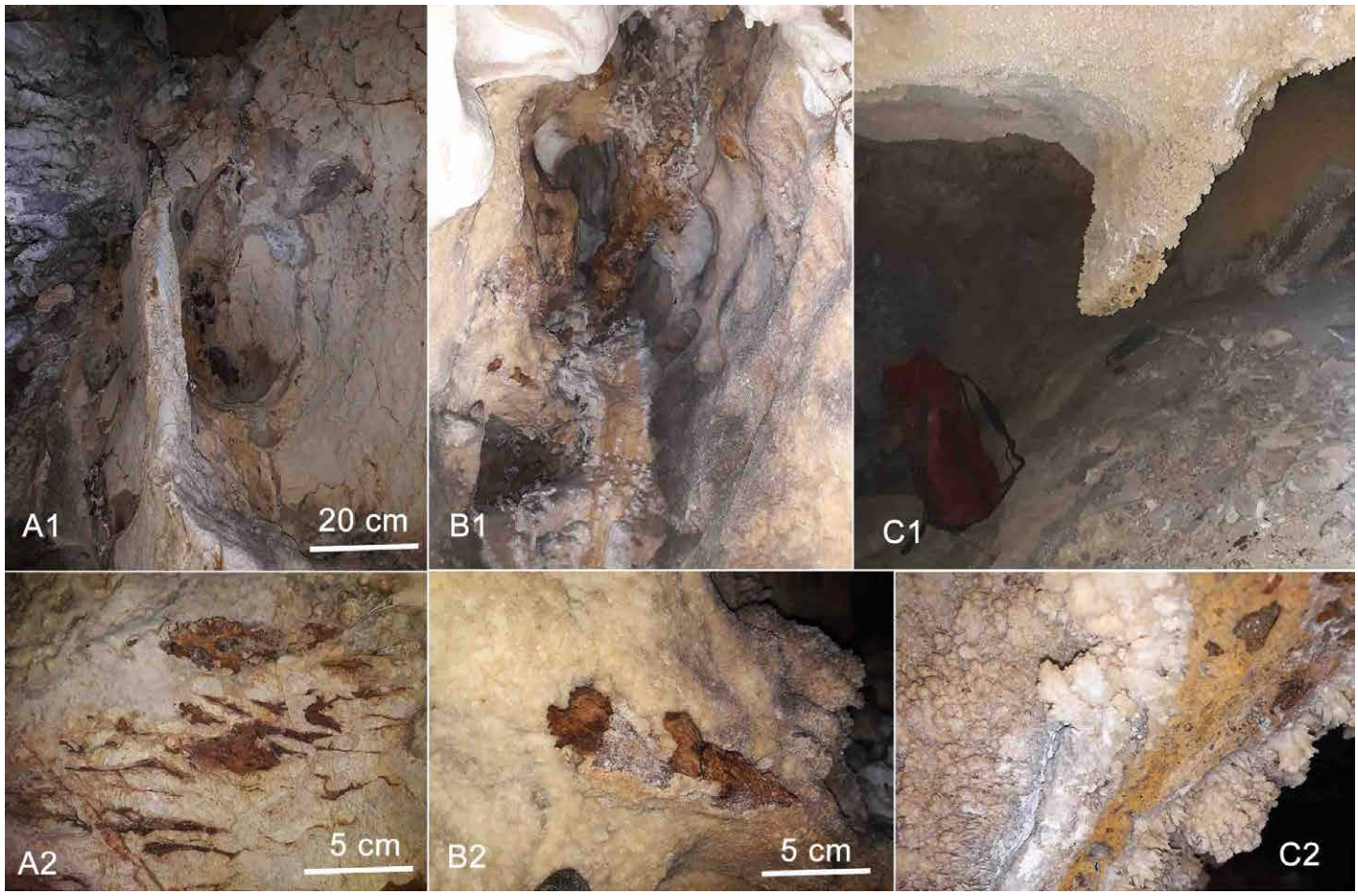

Figure 3. Photographs of iron oxide crust occurrences in Maronia Cave. (A1, A2) Sampling site Sp55. (B1, B2) Sampling site Sp56. (C1, C2) Sampling site Sp57 in a pendant covered by carbonate coralloids, crusts, and coatings. Fig. A2, B2, and C2 each show the crust in greater detail.

found. We chose three locations for sampling that were spread along the north half of the cave (Figs. 2 and 3). The first two samples come from cupola-shaped areas of the cave ceiling and from the sidewalls of these sites. The third sample was collected from a pendant that is covered with coralloids. Below the coralloids there is a massive iron oxide crust.

MVQ Cave (Fig. 4) was discovered by quarrying at the Mavros Vrachos hill about 220 m MSL in the southwestern part of the northeast-southwest striking Krousovitis Basin in the Serres region, northern Greece. This basin is filled with Neogene and Quaternary sediments (Karistineos, 1984) overlying mainly gneisses and marbles that belong to the Rhodope Massif of the Hellenides and granitoid intrusions of Tertiary age (e.g., granites, granodiorites, etc.). Travertine deposits occur in several locations in the basin.

In the entrance area of MQV Cave are two vertical passages, divided by a conical breccia deposit, forming in total a breccia pipe morphology. The southern passage is about 8 m in depth and choked by autochthonous sediments. The northern passage is about 20 m deep and connects to the main cave chamber. A 40 m long passage starts vertically from the east side of the chamber. It is inclined and stops at a small lake 56 m below the entrance elevation. This passage extends underwater for more than 10 m where two almost-vertical passages are developed more deeply. Another vertical passage starts at the southern part of the main chamber and is connected to small horizontal and vertical passages about 40–50 m below the entrance level. The deepest parts are narrow and inaccessible.

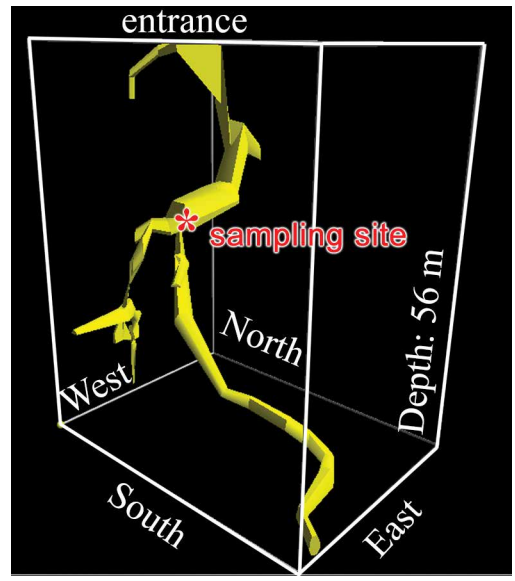

Figure 4. Block diagram of Mavros Vrachos Quarry Cave. Sampling site is depicted.

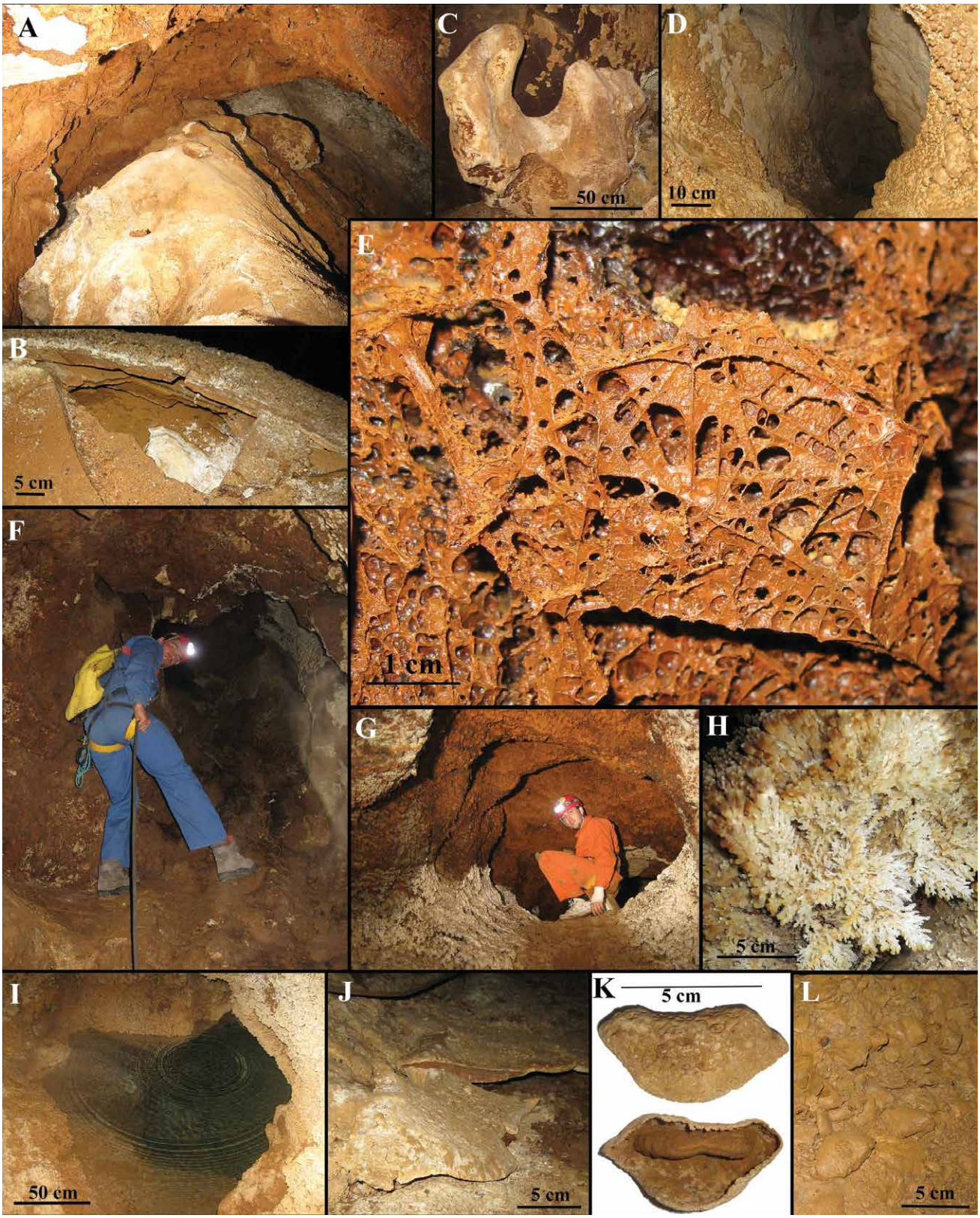

Figure 5. Photographs inside Mavros Vrachos Quarry Cave. (A) The main chamber covered by the iron oxide crust and view of the sedimentary ridge along its axis. (B) Details of broken layers in the ridge of the main chamber. (C) Dissolution remnant on the floor of the southern passage. (D) Feeder conduit at the south part of the cave. (E) Detail of the spongework structure of the iron oxide crust. (F) The vertical passage that connects the eastern conduit to the main chamber. (G) Part of the eastern conduit with symmetrical cross-section covered by the iron oxide crust and frostwork-coralloid alternations at the lower half of the passage. (H) Detail of the frostwork and coralloids. (I) The lake that is formed at the deepest part of the cave, 56 m below the entrance elevation. (J) Mudstones in proximity to the lake. (K, L) Detail of cave caps formed on mud nodules and in situ, respectively. Scale bars differ for each photograph.

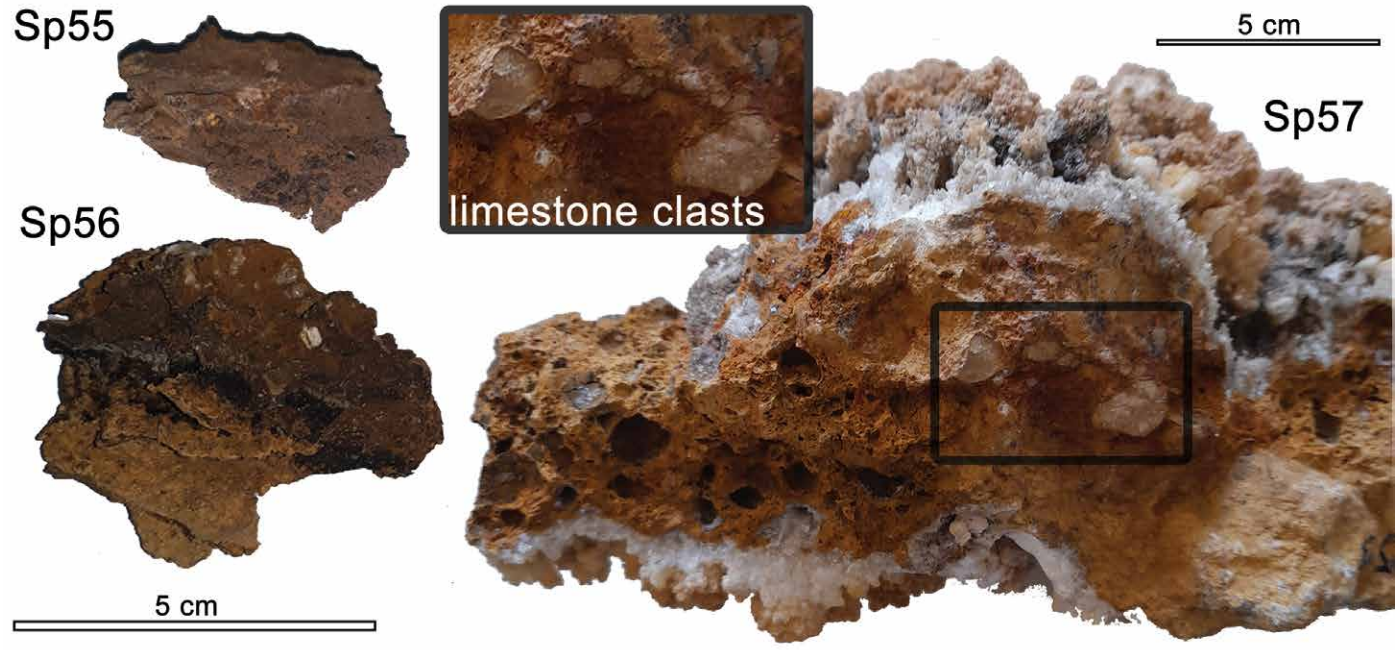

Figure 6. Macroscopic appearance of the examined iron oxide crusts from Maronia Cave. (Sp55, Sp 56, Sp57) Sample from the corresponding sites shown in Fig. 2. (Limestone clasts) Detail from the sample from site Sp57. Lower left scale bar applies to the samples from sites Sp55 and Sp56. Upper right scale bar applies to the sample from site Sp57 (except the limestone clasts detail).

An iron oxide crust a few centimeters thick (5–10 cm) covers most of the cave interior, and a few other speleothems are found, such as calcite spar consisting of a few millimeter-long crystals, carbonate crusts and aragonite and calcite frostwork alternating with globular coralloids, cave powder (Hill and Forti, 1997), and some mud nodules partially covered by a calcite layer resembling cave caps (Fig. 5J–L). The calcite spar is widespread within the cave in small pockets of the iron oxide crust. A ridge that consists of successive carbonate crusts (in at least the uppermost 10 cm) forms the cave floor along the long axis of the main chamber. This is the second most common type of speleothem in the cave due to its extent, after the iron oxide crusts. Its layers are not horizontally deposited, but instead, they follow the inclination of the ridge surface. Above the ridge there are no stalactites or any dripping sites. In general, dripping speleothems are almost absent. The alternation of frostwork and coralloids occur in the central chamber and the east passage, where it is delimited at the lowest parts of the passage. Cave powder and cave caps are found at the small lake in the deepest part of the cave and are related to its surface and its area of seasonal fluctuations. One sample of the iron oxide crust was collected from the main chamber of the cave for further investigation.

METHODS

Morphological and chemical investigation of iron oxide crust samples were carried out at the Scanning Microscope Laboratory, Aristotle University of Thessaloniki, using a JEOL Ltd. JSM840A SEM equipped with an energy-dispersive spectrometer with a 20 kV accelerating

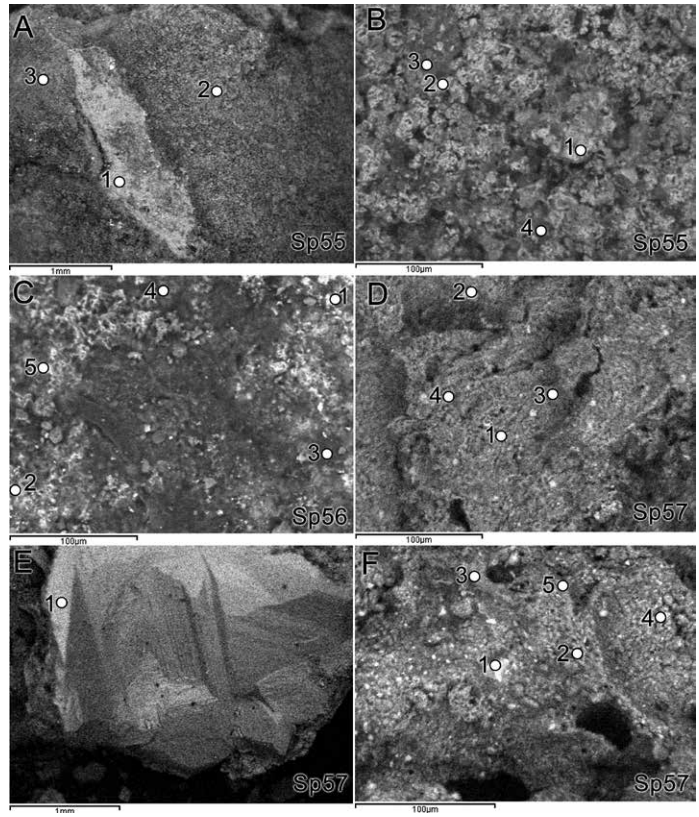

Figure 7. Backscattered SEM images of iron oxide crust samples from Maronia Cave. Numbered white circles correspond to the elemental composition sites provided in Table 1. (A, B) Sample Sp55 where mainly iron oxides and iron hydroxides are observed. (C) Sample Sp56. (C1) Iron oxides and iron hydroxides. (C2–C5) Aluminosilicates. (D, F) Sample Sp57 with iron oxides, iron hydroxides, and aluminosilicates. (E) Sample Sp57 with calcite. Scale bars correspond to the images above each bar.

Table 1. Elemental composition of the studied sample sites from Maronia Cave from Energy Dispersive Spectroscopy in weight percent (see Fig. 7).

Element	Sample Sp55						
	A1	A2	A3	B1	B2	B3	B4
Al	···	···	···	5.29	1.02	···	···
Si	···	3.81			2.66	17.74	···
Ca	···	3.38	1.83	18.02	2.09	12.07	2.85
Mn	···	···	···	21.16	···	···	···
Fe	77.73	67.73	75.74	29.13	60.02	35.10	74.63
As	···	···	···	···	9.27	···	···
O	22.27	25.09	22.43	26.41	24.94	35.08	22.52
Total	100.00	100.00	100.00	100.00	100.00	100.00	100.00

	Sample Sp56				
Element	C1	C2	C3	C4	C5
Mg	···	···	···	···	2.97
Al	···	2.97	4.98	4.23	2.88
Si	···	3.98	20.17	13.97	2.09
P	···	···	5.02	···	···
S	···	···	1.92	···	···
Ca	···	···	3.16	···	1.64
Fe	77.73	66.75	20.78	48.28	64.41
As	···	···	···	···	···
O	22.27	26.30	43.97	33.52	26.01
Total	100.00	100.00	100.00	100.00	100.00

	Sample Sp57									
Element	D1	D2	D3	D4	E1	F1	F2	F3	F4	F5
Mg	1.88	0.30	···	···	···	2.46				
Al	1.17	3.77	···	8.94	···	5.36	14.01	8.33	14.96	12.72
Si	2.78	5.62	19.74	28.95	···	8.88	20.27	36.26	23.58	31.77
K	···	···	···	···	···	···	0.86	1.29	0.86	0.74
Ti	···	···	···	···	···	···	9.45	···	···	···
P	···	3.08	···	···	···	···	···	···	···	···
Ca	···	7.48	···	4.49	71.47	···	···	···	0.02	···
Fe	68.97	48.84	44.91	11.58	···	51.92	10.40	3.99	15.73	5.52
O	25.20	30.91	35.35	46.04	28.53	31.38	45.02	50.13	44.86	49.25
Total	100.00	100.00	100.00	100.00	100.00	100.00	100.00	100.00	100.00	100.00

voltage and a 0.4 mA probe current. Pure cobalt was used as an optimization element. For SEM observations, the samples were coated with carbon (to an average thickness of 20 nm) using a vacuum evaporator JEOL-4X. Energy-dispersive X-ray spectroscopy analysis allows the chemical determination of phases with a size as small as 1 × 1 μm. In total, three representative sub-samples from the samples from sites Sp55, Sp56, and Sp57 in Maronia Cave were investigated as well as 1 sub-sample from the MVQ Cave sample.

RESULTS

In Maronia Cave, the first 2 samples are macroscopically similar (Fig. 6), with Sp55 and Sp56 consisting of massive porous areas and crusts. Both samples show dark red to brown color while sample Sp57 is more massive, porous, and lighter in color. Upon close examination of the external part of the sample that is covered with coralloids, its pores are

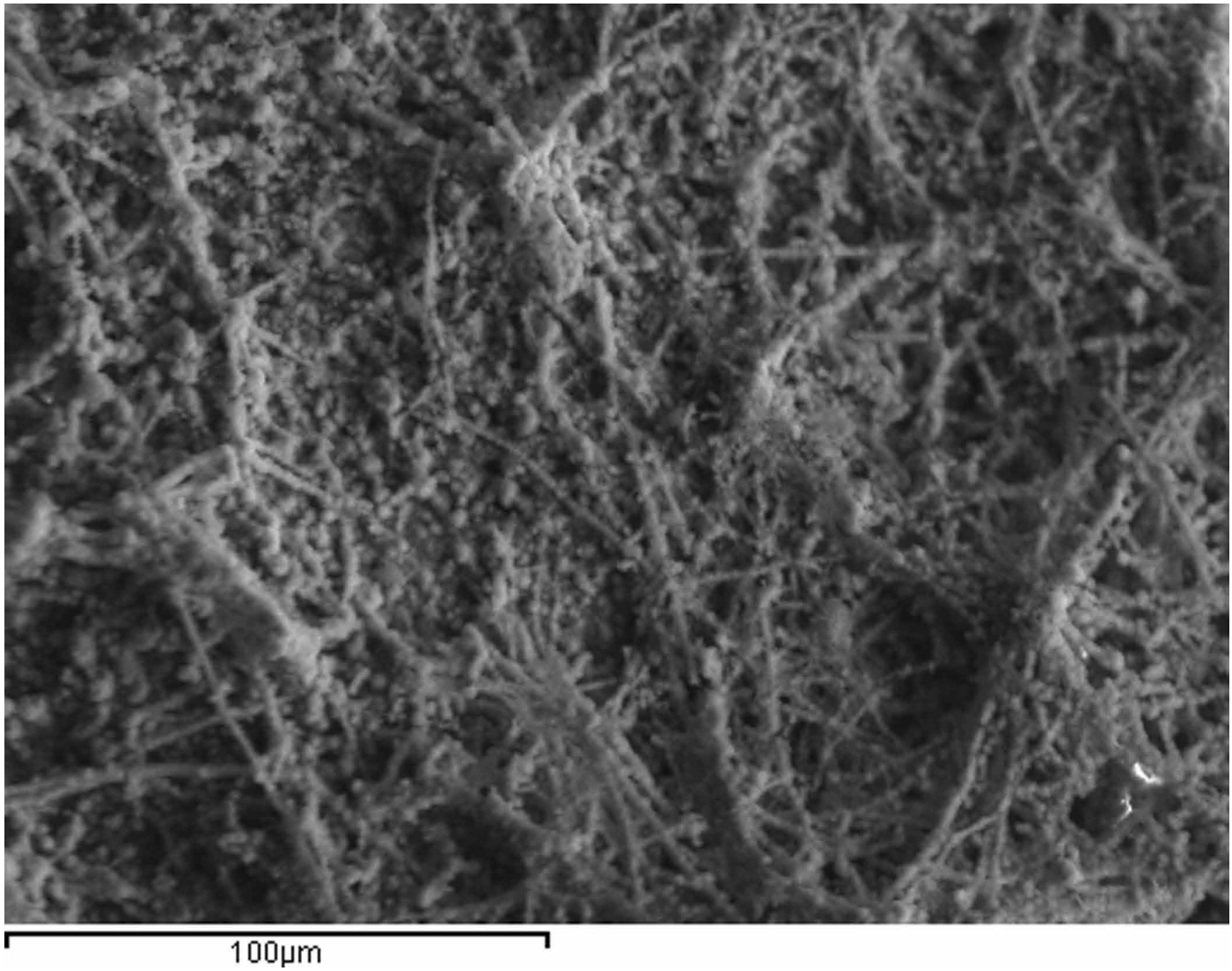

Figure 8. Backscattered SEM image from the iron oxide crust in Mavros Vrachos Quarry Cave where a network of tiny filaments is observed. Scale bar shown below image.

found to be lined with small euhedral calcite crystals. Some small fragments of limestone, in the shape and size of the pores, are found in areas where large pores are missing.

With the SEM (Fig. 7), sample Sp55 appears to consist of micrometer-sized crystals and aggregates, and the surface exhibits pores that are about 10 μm in size. The maximum iron content is 78 % by weight, which is consistent for iron oxide minerals such as goethite, hematite, and magnetite. In one subsampling point, manganese replaces the iron content. Other elements found are aluminum, silicon, calcium and arsenic. Similarly, sample Sp56 also has a high iron content of about 78 %. Places with a lower content of iron display higher amounts of silica and other elements such as aluminum, magnesium, calcium, phospherous, and sulfur. It also consists of small grains (about 15μm in diameter) and massive areas. The third sample, Sp57, displays lower iron content that reaches 69 %, where calcium carbonate and aluminosilicate minerals make up a small percent of the crust. Apart from iron, calcium, silicon, and aluminum, other elements found in this sample include magnesium, potassium, phospherous, and titanium. Although macroscopically it appears more porous, it looks relatively massive in the SEM. Grains of aluminosilicates are only a few micrometers in diameter, whereas calcite crystals are few millimeters in diameter. The results of chemical analyses for these samples are summarized in Table 1.

The sample from MVQ Cave (Fig. 8) is much more porous than the samples from Maronia Cave and very fragile. Its color is more or less similar to the other iron oxide crusts along the cave's length or depth. The analyzed sample consists mainly of iron, which reaches 96 % by weight (Table 2). Its structure observed in the SEM consists of tiny filaments that are oriented at every direction forming a network structure. The filaments consist of spherical aggregates with 1–5 μm radii. These spherical aggregates consist of needle-like crystallites that are radially arranged.

Table 2. Mean values and range of elements in weight % found in the Fe-oxide crust from Mavros Vrachos Quarry Cave.

Element	Mean	Min	Max
O	27.33	2.96	36.70
Na	0.99	0.99	0.99
Mg	0.53	0.49	0.58
Al	1.29	0.32	2.15
Si	3.48	0.53	4.54
Ca	0.35	0.22	0.62
Fe	67.43	56.35	96.19
Total	100.00	N.A.	N.A.

DISCUSSION

Both caves sampled in this study have been included in the list of hypogene or possibly hypogene caves in Greece (Lazaridis, 2017). Various occurrences of iron oxides and iron hydroxides in hypogene caves under a number of conditions are summarized in Table 3. Both subaerial and subaqueous conditions have been found to be responsible for the formation of these deposits. Manganese-rich deposits may be associated with the iron oxides. The spongy porous appearance might be associated with microbial activity. In general, iron and manganese are mobilized from mineralizations in the host rock (Gázquez et al., 2011, 2012a, 2012b) or from dissolution of trace elements in the vadose parts of caves (Spilde et al., 2006). Although ferromanganese deposits in the caves of the Guadalupe Mountains (USA) have been considered the residue of dissolution during speleogenesis (Davis, 2000; Polyak and Provencio, 2001) or thought to be formed by condensation corrosion (Queen, 1994), the enrichment of iron and manganese oxides remains problematic. However, it could be explained by a microbe-driven process modeled by a number of studies (Northup et al., 2000, 2003; Boston et al., 2001; Spilde et al., 2005, 2006).

The iron oxide crusts in Maronia Cave form two different types: one type covers sidewalls and the other is found as a pendant-like ceiling protrusion. The first type displays higher iron content and fills small discontinuities and voids on

Table 3. Hypogene caves with Fe-oxides and hydroxides and their main characteristics.

Cave/Country	Type of Deposit	Associated with	Conditions	Reference
Mavros Vrachos Quarry Cave, Greece	Spongy texture with microbial filaments	Symmetrical passages, feeders, cupolas	Hypogene/ hydrothermal speleogenesis, subaqueous formation	Present work
Maronia Cave, Greece	Porous crust	Pendant forms, discontinuities, cupolas	Possibly Hypogene speleogenesis	Present work
Iboussières Cave, France	Spongy microbial ferruginous material	Vertical wall channel “black tubes”	Hypogene speleogensis	Audra et al., 2017
Rhar Medjraba, Algeria	Spongy texture	Microbial mats	Hypogene/ sulfuric acid speleogenesis	Coiait and Quinif, 1978
El-Balayza Caves, Egypt	Iron oxides	Manganese oxides and feeder morphology	Hypogene speleogenesis	Mostafa, 2012
Cave in southwestern Sardinia, Italy	Iron oxides	...	Subaerial formation by water films	De Waele et al., 2017
Cave of the Winds and Glenwood Caverns, Colorado, USA	Spongy texture with bacteria filaments or small uniform grains (1–2 μm)	Iron oxide mammillaries of inorganic origin/ breccias/ calcite	Hypogene speleogenesis/ subaqueous formation	Luiszer, 1994; Maslyn et al., 2017
Lechuquilla Cave, New Maxico, USA	Rusticles: “subaqueous streamers of iron mineral sheaths of iron-oxidizing bacteria”	Calcite crust	“reduced iron-rich fluid was trickling from above into standing water”	Davis, 2000
Mbobo Mkulu, South. Africa	Goethite speleothems on the ceiling	...	Dripping water/ subaerial formation	Martini, 2017
Caves of the Apennines Mountains, Italy	Goethite coatings	Presence of mineralized water	Hypogene speleogenesis	Galdenzi and Manichetti, 2017
Caves of the Buda thermal karst, Hungary	Iron hydroxide precipitates dominated by goethite	Cave rafts and discharge areas	Hypogene/ hydrothermal speleogenesis/ subaqueous formation	Mádl-Szonyi et al., 2017
Sima de la Higuera Cave, Spain	Ferromanganese oxyhydroxides	Botryoidal aggregates/ hydrothermal calcite veins/ related to boxwork pattern	Hypogene speleogenesis/ multiphase process of formation	Gázquez et al., 2012a
Germany	Goethite deposits	Siderite weathering	Hypogene speleogenesis	Kempe, 1971; Kempe et al., 2017
Warda, Northern Jordan	Karstic iron ore deposit	Calcite veins	Hypogene speleogenesis	Al-Malabeh et al., 2008

the walls and ceiling. By the term discontinuity, we mean any type of break in the rock, such as bedding planes, joints, faults, etc. These crusts cover the host rock in cupolas, indicating that the crust formed at or soon after the termination of speleogenesis. Regarding the second type, its extent and relation to the dissolution forms of the bedrock cannot be clearly observed due to speleothem coverage. It can be assumed that the presence of limestone clasts in the deposit indicates an early karstification filling of a discontinuity. Since the bedding planes are of low angle, a tectonic discontinuity can be suggested. This deposit was later exposed from dissolution that removed most of the limestone clasts, reshaped the passage and left the iron-rich filling as an undissolved remnant.

In MVQ Cave the deposition of the various carbonate speleothems is related to distinct conditions. The calcite spar seems to be related to the formation conditions of the iron oxide crust. It is contemporaneous or follows its deposition since it appears to either be covered by or to cover the iron oxide deposits. The formation of the carbonate crusts and the ridge in the central chamber is enigmatic. Any relation to dripping water or flowing water is excluded because of its location and shape, respectively. So, most probably it is related to subaqueous formation conditions, and as it can be supposed from its distance from the sidewalls at the west side and around the passages, its shape is affected by rising water inputs in the chamber. This assumption is worthy of further investigation. The deposition of frostwork is related to subaerial capillary films, and for its growth there are several prerequisites concerning the cave environment, the bedrock and the rate and chemistry of the seeping water (Hill and Forti, 1997, and references therein). It is common for frostwork to alternate with coralloids (popcorn) due to admixtures in solution or to changes in speed of crystallization. Frostwork and coralloids from MVQ Cave have been developed on the iron oxides, which have high porosity (a spongework pattern), fine filamentous textures, and the resistance of the goethite to solution by capillary films. Due to these characteristics, they are ideal bedrock (according to the conditions considered by Coudray and Cabral, 1978a, 1978b) for the formation of frostwork and coralloids. Coralloids from MVQ Cave consist of calcite and aragonite. The deposition of aragonite is preferable under evaporative conditions, which, along with the presence of air flow, is favorable for the growth of frostwork. However, the existence of air flow inside MVQ Cave is not strong, and it is questionable if it existed before the artificial entrance. Finally, the cave powder and the cave caps are related to the conditions that are presently found in the deepest part of the cave associated with stagnant water. Speleothems that are related to seeping water (e.g., stalactites) are almost completely absent indicating a restricted entrance and recharge from surface above the cave and/or an effective sealant above the cave.

The iron oxide crust in MVQ Cave appears to have been formed subaqueously due to its presence in the whole known extent of the cave and its similar thickness throughout the cave. It is also formed inside all the dissolution forms of small-scale morphology that are indicative of the presence of rising water conditions, suggesting a probable deposition during the latest stages of speleogenesis. SEM observation shows that its fragile structure resembles structures formed by microorganisms (Fig. 8).

CONCLUSIONS

The four samples examined here can be considered as three different types of Maronia and MVQ Cave iron oxide crusts: high iron content crust with some porosity and formation on host rock surface and discontinuities; high iron content but lower than the first type, that include limestone clasts and pores originating from dissolved clasts; and a high iron content, significantly porous crust that is formed by a network of filaments that indicate microbial activity. The 1st type is considered co- or post-dissolutional since it covers cupolas. The second type, which developed secondary porosity due to dissolution of clasts, seems to have undergone a phase of dissolution that also formed the passage in a way that left behind the insoluble iron crust that was filling some early void. The third type is subaqueous and most apparently phreatic due to its extent and isotropic deposition. It is the dominant speleothem in MVQ Cave and a small number of other speleothems are either related to its presence and capillary water flow or to the presence of stagnant water. All-in-all, vadose speleothems are almost absent in this cave, indicating a delimited vadose input and reinforcing the phreatic origin of the crusts. Oxidation might be related to microbial activity in this case, whereas for the first 2 types no evidence of such activity is observed. This type is worthy of study in further detail to investigate the conditions under which the cave and the crust were formed.

ACKNOWLEDGMENTS

Sampling was carried out under the authorization of the Ephorate of Paleoanthropology and Speleology, Greek Ministry of Culture and Sports. We thank two anonymous reviewers for their valuable comments that improved this paper.

REFERENCES

Al-Malabeh, A., Kempe, S., Henschel, H.-V., Hofmann, H., and Tobschall, H. J., 2008, The possibly hypogene karstic iron ore deposit of Warda near Ajloun (northern Jordan), its mineralogy, geochemistry, and historic mine: Acta Carsologica, v. 37, p. 241–253, https://doi.org/10.3986/ac.v37i2-3.149.

Audra, P., 2017a, Hypogene caves in France, *in* Klimchouk, A., Palmer, A.N., De Waele, J., Auler, A.S., and Audra, P., eds., Hypogene Karst Regions and Caves of the World: Cham, Switzerland, Springer, p. 61–83, https://doi.org/10.1007/978-3-319-53348-3_3.

Audra, P., 2017b, Hypogene Caves in North Africa (Morocco, Algeria, Tunisia, Libya, and Egypt), *in* Klimchouk, A., Palmer, A.N., De Waele, J., Auler, A.S., and Audra, P., eds., Hypogene Karst Regions and Caves of the World: Cham, Switzerland, Springer, p. 853–864, https://doi.org/10.1007/978-3-319-53348-3_58.

Audra, P., Barriquand, L., Bigot, J.-Y., Cailhol, D., Caillaud, H., Vanara, N., Nobécourt, J.-C., Madonia, G., Vattano, M., and Renda, M., 2016, L'impact méconnu des chauves-souris et du guano dans l'évolution morphologique tardive des cavernes [The unknown impact of bats and guano in the late morphological evolution of caves]: Karstologia, v. 68, p. 1-20, https://hal.science/hal-01838348.

Audra P., et al., 2017, Bat urea-derived minerals in arid environment: First identification of allantoin, $C_4H_6N_4O_3$, in Kahf Kharrat Najem Cave, United Arab Emirates: International Journal of Speleology, v. 46, p. 81–92, https://doi.org/10.5038/1827-806X.46.1.2001.

Boston, P.J., et al., 2001, Cave biosignatures suites: Microbes, minerals, and Mars: Astrobiology, v. 1, p. 25–55, https://doi.org/10.1089/153110701750137413.

Bruxelles, L., Jarry, M., Bigot, J.-Y., Bon, F., Cailhol, D., Dandurand, G., and Pallier, C., 2016. La biocorrosion, un nouveau paramètre à prendre en compte pour interpréter la répartition des œuvres parietals [Biocorrosion, a new parameter to consider to interpret the distribution of parietal artwork], Karstologia, v. 68, p. 21–30, https://hal.science/hal-01838098.

Cailhol, D., et al., 2019, The contribution of condensation-corrosion in the morphological evolution of caves in semi-arid regions: Preliminary investigations in the Kyrenia Range, Cyprus: Acta Carsologica, v. 48, p. 5-27, https://doi.org/10.3986/ac.v48i1.6782.

Coiffait, P.E., and Quinif, Y., 1978, Fracturation et karstification d'un massif: L'exemple de l'Azerou el Kebir (Algérie du nord) [Fracturization and karstification of a massif: The example of the Azerou el Kebir (Northern Algeria)], International Journal of Speleology, v. 10, p. 245–252, https://doi.org/10.5038/1827-806X.10.3.2.

Coudray, J., and Cabrol, P., 1978a, Les phénomènes de diagenèse dans les oncretions de grottes du sud de la France: Aragonisation de la calcite? [The phenomena of diagenesis in the cave concretions of southern France: Aragonization of calcite?]: Sixth Meeting of Carbonate Sedimentologists, Liverpool, Manuscript report, 3 p.

Coudray, J., and Cabrol, P., 1978b, Some new aspects of diagenesis in cave speleothems of Southern France, Sixth Meeting of Carbonate Sedimentologists, Liverpool, Abstract, 1 p.

Davis, D. G., 2000, Extraordinary features of Lechuguilla Cave, Guadalupe Mountains, New Mexico: Journal of Cave and Karst Studies, v. 62, p. 147-157, https://legacy.caves.org/pub/journal/PDF/V62/v62n2-Davis.pdf.

De Waele, J., Gázquez, F., Forti, P., and Naseddu, A., 2017, Inactive hydrothermal hypogenic karst in SW Sardinia (Italy), *in* Klimchouk, A., Palmer, A.N., De Waele, J., Auler, A.S., and Audra, P., eds., Hypogene Karst Regions and Caves of the World: Cham, Switzerland, Springer, p. 183-197, https://doi.org/10.1007/978-3-319-53348-3_11.

Dublyansky, Y.V., 2014, Hypogene speleogenesis—discussion of definitions, *in* Klimchouk, A., Sasowsky, I.D., Mylroie, J., Engel, S.A., and Engel, A.S., eds., Hypogene Cave Morpholgies: Leesburg Virginia, Karst Waters Institute, Special Publication 18, p. 1–3, https://karstwaters.org/wp-content/uploads/2015/04/SP18_Hypogene1.pdf.

Galdenzi, S., and Menichetti, M., 2017, Hypogenic caves in the Apennine Mountains (Italy), *in* Klimchouk, A., Palmer, A.N., De Waele, J., Auler, A.S., and Audra, P., eds., Hypogene Karst Regions and Caves of the World: Cham, Switzerland, Springer, p. 127–142, https://doi.org/10.1007/978-3-319-53348-3_7.

Gázquez, F., Calaforra, J.M., and Forti, P., 2011, Black Mn-Fe crusts as markers of abrupt palaeoenvironmental changes in El Soplao Cave (Cantabria, Spain): International Journal of Speleology, v. 40, p. 163–169, https://doi.org/10.5038/1827-806X.40.2.8.

Gázquez, F., Calaforra, J.-M., and Rull, F., 2012a, Boxwork and ferromanganese coatings in hypogenic caves: An example from Sima de la Higuera Cave (Murcia, SE Spain): Geomorphology, v. 177–178, p. 158–166, https://doi.org/10.1016/j.geomorph.2012.07.022.

Gázquez, F., Calaforra, J.-M., Forti, P., Rull, F., and Martínez-Frías, J., 2012b, Gypsum-carbonate speleothems from Cueva de las Espadas (Naica mine, Mexico): Mineralogy and palaeohydrogeological implications: International Journal of Speleology, v. 41, p. 211–220, https://doi.org/10.5038/1827-806X.41.2.8.

Hill, C., and Forti, P., 1997, Cave Minerals of the World, 2nd ed., Huntsville, Alabama, National Speleological Society, 463 p.

Karistineos, N., 1984, Palaeogeographic evolution of the Serres Basin: Lithostratigraphy, biostratigraphy, tectonics [Ph.D. dissertation], Aristotle University of Thessaloniki, Greece, 230 p.

Kempe, S., 1971, Speläogenetisch wirksames CO_2 durch Verwitterung von Siderit? [Speleogenetically effective CO_2 from weathering of siderite?]: Verband der Deutschen Höhlen- und Karstforscher e.V. München, Mitteilungen, v. 18, p. 38, https://www.researchgate.net/publication/232804666_Spelaogenetisch_wirksames_CO2_durch_Verwitterung_von_Siderit.

Kempe, S., Bauer, I., and Glaser, S., 2017, Hypogene caves in Germany, geological and geochemical background, *in* Klimchouk, A., Palmer, A.N., De Waele, J., Auler, A.S., and Audra, P., eds., Hypogene Karst Regions and Caves of the World: Cham, Switzerland, Springer, p. 329–347, https://doi.org/10.1007/978-3-319-53348-3_21.

Klimchouk, A., 2017, Types and settings of hypogene karst, *in* Klimchouk, A., Palmer, A.N., De Waele, J., Auler, A.S., and Audra, P., eds., Hypogene Karst Regions and Caves of the World: Cham, Switzerland, Springer, p. 1–39, https://doi.org/10.1007/978-3-319-53348-3_1.

Kouris, Ch., 1980. Geologic map of Greece, Mesi-Xylagani sheet, Institute of Geology and Mineral Exploration of Greece, scale 1:50,000, 1 sheet.

Lazaridis, G., 2005. Observations on the shields of the Cyclop Polyphemus Cave—Maronia (Thrace, Greece): Bulletin of Geological Society of Greece, v. 37, p. 168-178.

Lazaridis, G., 2017, Hypogene speleogenesis in Greece, *in* Klimchouk, A., Palmer, A.N., De Waele, J., Auler, A.S., and Audra, P., eds., Hypogene Karst Regions and Caves of the World: Cham, Switzerland, Springer, p. 225-239, https://doi.org/10.1007/978-3-319-53348-3_14.

Luiszer, F.G., 1994, Speleogenesis of Cave of the Winds, Manitou Springs, Colorado, *in* Sasowsky, I.D., and Palmer, M.V., eds, Breakthroughs in Karst Geomicrobiology and Redox Geochemistry, Charles Town, West Virginia, Karst Waters Institute, Special publication 1, p. 91–109, https://karstwaters.org/publications/sp1-breakthroughs-in-karst-geomicrobiology-and-redox-geochemistry/.

Mádl-Szőnyi, J., Erőss, A., and Tóth, Á, 2017, Fluid flow systems and hypogene karst of the Transdanubian Range, Hungary—with special emphasis on Buda thermal karst, *in* Klimchouk, A., Palmer, A.N., De Waele, J., Auler, A.S., and Audra, P., eds., Hypogene Karst Regions and Caves of the World: Cham, Switzerland, Springer, p. 267–278, https://doi.org/10.1007/978-3-319-53348-3_17.

Martini, J., 2017, Hypogene Karst in Southern Africa, *in* Klimchouk, A., Palmer, A.N., De Waele, J., Auler, A.S., and Audra, P., eds., Hypogene Karst Regions and Caves of the World: Cham, Switzerland, Springer, p. 865-878, https://doi.org/10.1007/978-3-319-53348-3_59.

Maslyn, R.M., DuChene, H.R., and Luiszer, F.G., 2017, Structural Settings and Hypogenic Flow Paths for Three Colorado Caves, *in* Klimchouk, A., Palmer, A.N., De Waele, J., Auler, A.S., and Audra, P., eds., Hypogene Karst Regions and Caves of the World: Cham, Switzerland, Springer, p. 575–590, https://doi.org/10.1007/978-3-319-53348-3_36.

Melfos, B.I., 1995, Investigations of the base and precious metals of the Circum Rhodope Belt in Thrace [Ph.D. thesis], Aristotle University of Thessaloniki, School of Geology, 289 p., https://ikee.lib.auth.gr/record/130758/files/.

Melfos, B., Chatzipetros, A., Chatzopoulou, A., Vasiliadou, A., Lazaridis, G., Vaxevanopoulos, M., Syrides, G., Tsoukala, E., and Pavlides, S., 2005, Geological, petrographical, and palaeonotological study of the Maronia cave in the Eocene, nummulitic limestone of western Thrace: Bulletin of the Geological Society of Greece, v. 37, p. 153-167, http://geolib.geo.auth.gr/index.php/bgsg/article/view/1220/1090.

Mostafa, A.A.-F., 2012, Caves of the Nile Valley (Governorate of Assiut, Middle Egypt): A long-term interaction between human societies and their environment: Géomorphologie, v. 18, p. 37–44, https://doi.org/10.4000/geomorphologie.9719.

Northup, D.E., Barns, S.M., Yu, L.E., and Spilde, M., 2003, Diverse microbial communities inhabiting ferromanganese deposits in Lechuguilla and Spider Caves: Environmental Microbiology, v. 5, p. 1071–1086, https://doi.org/10.1046/j.1462-2920.2003.00500.x.

Northup, D.E., Dahm, C.N., Melim, L.A., Spilde, M.N., Crossey, L.J., Lavoie, K.H., Mallory, L.M., Boston, P.J. Cunningham, K.I., and Barns, S.M., 2000, Evidence for geomicrobiological interactions in Guadalupe caves: Journal of Cave and Karst Studies, v. 62, p. 149–160, https://legacy.caves.org/pub/journal/PDF/V62/v62n2-Northup.htm.

Onac, B.P., Pedersen, R.B., and Tysseland, M., 1997, Presence of rare-earth elements in black ferromanganese coatings from Vântului Cave (Romania): Journal of Cave and Karst Studies, v. 59, p. 128–131, https://legacy.caves.org/pub/journal/PDF/V59/V59N3-Onac.pdf.

Onac, B.P., and Forti, P., 2011, Minerogenetic mechanisms occurring in the cave environment: An overview: International Journal of Speleology, v. 40, p. 79–98, https://doi.org/10.5038/1827-806X.40.2.1.

Papadopoulos, P., 1982, Geologic map of Greece, Maronia sheet, Institute of Geology and Mineral Exploration of Greece, scale 1:50,000, 1 sheet.

Panti, A, 2015, Light in the cave of Maronia: Lamps from the archaic to byzantine times, *in* Proceedings of the Balkan Light Conference 2015, 16-19 September 2015, Athens, Greece, p. 229–236, https://www.academia.edu/17715380/Light_in_the_cave_of_Maronia_Lamps_from_the_archaic_to_byzantine_times_in_Balkan_Light_Conference_Athens_16_18_09_2015_229_236.

Pavlides, S., Tsoukala, E., Chatzipetros, A., Chatzopoulou, A., Melfos, V., Vasileiadou, A., Lazarides, G., and Vaxevanopoulos, M., 2005, The Maronia cave in the ummulitic limestone (Thrace, Greece): Geology & Palaeontology: Proceedings of 14th International Congress of Speleology, 21–28 August 2005, Kalamos, Hellas, v. 1, p. 88–90, https://digitalcommons.usf.edu/cgi/viewcontent.cgi?article=1118&context=kip_talks.

Petrocheilou, A, 1984, The Greek Caves: Athens, Ekdotike Athenon, 160 p.

Polyak, V.J., Provencio, P., 2001, By-product materials related to H_2S-H_2SO_4 influenced speleogenesis of Carlsbad, Lechuguilla, and other caves of the Guadalupe Mountains, New Mexico: Journal of Cave and Karst Studies, v. 63, p. 23–32, https://legacy.caves.org/pub/journal/JCKS/PDF/V63/v63n1-Polyak.pdf.

Queen, J.M, 1994. Influence of thermal atmospheric convection on the nature and distribution of microbiota in cave environments, *in* Sasowsky, I.D., and Palmer, M.V., eds, Breakthroughs in Karst Geomicrobiology and Redox Geochemistry, Charles Town, West Virginia, Karst Waters Institute, Special publication 1, p. 62–64, https://karstwaters.org/publications/sp1-breakthroughs-in-karst-geomicrobiology-and-redox-geochemistry/.

Spilde, M.N., Northup, D.E., and Boston, P.J., 2006, Ferromanganese Deposits in the Caves of the Guadalupe Mountains, *in* Land, L., Lueth, V.W., Raatz, W., Boston, P., Love, D.L., eds., Caves and Karst of Southeastern New Mexico, New Mexico Geological Society 57th Annual Field Conference, September 21–24, 2006, p. 161–166, https://doi.org/10.56577/FFC-57.161.

Spilde, M.N., Northup, D.E., Boston, P.J., Schelble, R.T., Dano, K.E., Crossey, L.J., and Dahm, C.N., 2005, Geomicrobiology of cave ferromanganese deposits: A field and laboratory investigation: Geomicrobiology Journal, v. 22, p. 99–116, https://doi.org/10.1080/01490450590945889.

Sylaiou, S., Georgiadis, Ch., Panti, A., and Patias, P., 2009, Recording of cultural and natural heritage with ground-based laser scanning: The case of the Maroneia Cave, *in* Tsipopoulou, M., ed., Proceedings of the International Conference, Digital Heritage in the New Knowledge Environment: Shared Spaces and Open Paths to Cultural Content, Athens, October 31–November 2, 2008, p. 52–54.

Vaxevanopoulos, M., and Melfos, V., 2010. Hypogenic features in Maronia Cave, Thrace, Greece: Evidence from morphologies and fluid inclusions: Bulletin of the Geological Society of Greece, v. 43, p. 948–957, https://doi.org/10.12681/bgsg.11260.